Alternating-laser excitation

Hohlbein, Johannes; Craggs, Timothy D.; Cordes, Thorben

Published in:
Chemical Society Reviews

DOI:
10.1039/c3cs60233h

Publication date:
2014

Chem Soc Rev

REVIEW ARTICLE

View Article Online
View Journal | View Issue

Cite this: *Chem. Soc. Rev.*, 2014, **43**, 1156

Alternating-laser excitation: single-molecule FRET and beyond

Johannes Hohlbein,*[a] Timothy D. Craggs[b] and Thorben Cordes[c]

Received 3rd July 2013

DOI: 10.1039/c3cs60233h

www.rsc.org/csr

The alternating-laser excitation (ALEX) scheme continues to expand the possibilities of fluorescence-based assays to study biological entities and interactions. Especially the combination of ALEX and single-molecule Förster Resonance Energy Transfer (smFRET) has been very successful as ALEX enables the sorting of fluorescently labelled species based on the number and type of fluorophores present. ALEX also provides a convenient way of accessing the correction factors necessary for determining accurate molecular distances. Here, we provide a comprehensive overview of the concept and current applications of ALEX and we explicitly discuss how to obtain fully corrected distance information across the entire FRET range. We also present new ideas for applications of ALEX which will push the limits of smFRET-based experiments in terms of temporal and spatial resolution for the study of complex biological systems.

Introduction

The study of physical and biological processes on the molecular level relies on the continuous development and improvement of sophisticated instrumentation and analytical methods. Whereas X-ray crystallography and Nucleic Magnetic Resonance (NMR) were, and still are, essential for resolving the atomic structure of biomolecules, they are less suited for studying the complex and often dynamic interactions within and between those molecules. During the past twenty years, a wide range of fluorescence-based methods have been developed with the prospect of probing molecular structure, dynamics and interactions at unprecedented spatial and temporal resolution.[1–9] A hallmark of many of these methods is the possibility to overcome the ensemble- and time-averaging inherent to conventional biochemical techniques, which often obscure the identification and interpretation of asynchronous reactions, transient conformational states, and rare sub-species. This review will focus on a technique known as alternating-laser excitation (ALEX),[10] which was initially developed as an extension of

[a] *Laboratory of Biophysics, Wageningen UR, Wageningen, The Netherlands. E-mail: Johannes.Hohlbein@wur.nl; Fax: +31 317 482 725; Tel: +31 317 482 635*
[b] *Department of Physics, University of Oxford, Oxford, UK*
[c] *Molecular Microscopy Research Group and Single-molecule Biophysics, Zernike Institute for Advanced Materials, University of Groningen, Groningen, The Netherlands*

Johannes Hohlbein

Johannes Hohlbein is an Assistant Professor in the Laboratory of Biophysics at Wageningen University (The Netherlands). He obtained his PhD from the Martin Luther University Halle-Wittenberg and has worked for several years as a Postdoctoral Research Fellow in the group of Prof. Achilles Kapanidis at the University of Oxford (UK). His current research focuses on studying DNA–protein interactions and especially DNA-processing enzymes. Other research interests include the study of transcription factors and steroid receptors in Arabidopsis thaliana using single-molecule techniques.

Timothy D. Craggs

Timothy Craggs is a Postdoctoral Research Fellow in the Gene Machines Group, headed by Prof. Achillefs Kapanidis, at the University of Oxford. Having gained his PhD in Biophysics from the University of Cambridge, he worked on DNA replication and repair at the University of St Andrews, before winning a Lindemann Trust Fellowship to Yale University in 2010. His current research interests include developing single-molecule fluorescence techniques for structural biology and the role of conformational dynamics in enzyme catalysis, exemplified by DNA replication and repair proteins and their substrates.

single-molecule Förster Resonance Energy Transfer (smFRET).[11] Besides providing an ideal framework for FRET-based, accurate monitoring of distances between two fluorophores in the 2–10 nm range, the ALEX scheme can also be used in applications which do not necessarily require the presence of FRET such as biosensing.[12]

Theory and methodological background

Single-molecule FRET (smFRET)

FRET describes a distance-dependent and non-radiative energy transfer from a high-energy fluorophore (donor) to a lower-energy chromophore (acceptor), which is often also a fluorophore. FRET can occur if three conditions are fulfilled: (1) the emission spectrum of the donor overlaps with the absorption spectrum of the acceptor, (2) both fluorophores are in close proximity, *i.e.*, at a distance of 2–10 nm, and (3) the dipole moments of both fluorophores are not perpendicular to each other.[13–15]

The FRET efficiency E can be expressed in terms of two rate constants. These relate to the fluorescence lifetime of the donor in the absence of the acceptor ($k_D = \tau_D^{-1}$) and the energy transfer rate between the donor and the acceptor (k_T). E is hence easily determined by comparing the fluorescence lifetimes τ_D of the donor-only species and $\tau_T^{-1} = k_D + k_T = \tau_D^{-1} + k_T$ for the donor–acceptor species. Förster showed that the transfer efficiency E is inversely proportional to the sixth power of the distance R between the two dipoles

$$E = \frac{k_T}{k_T + k_D} = 1 - \frac{\tau_T}{\tau_D} = \frac{1}{1 + (R/R_0)^6}. \quad (1)$$

Here, R_0 is the Förster radius which describes the donor-to-acceptor distance at which the FRET efficiency equals 50%. We calculate R_0 using

$$R_0^6 = \frac{9000 \ln 10 \Phi_D \kappa^2}{128\pi^5 N n^4} \int_0^\infty f_D(\lambda)\varepsilon_A(\lambda)\lambda^4 \, d\lambda, \quad (2)$$

Thorben Cordes

Thorben Cordes is an Assistant Professor of "Super-Resolution Microscopy" at the Zernike Institute for Advanced Materials at the University of Groningen (The Netherlands). He obtained his PhD from the LMU Munich (Germany) and was a postdoctoral researcher in Munich and Oxford (UK). His research group "Molecular Microscopy" focuses on the development and application of novel fluorescence-based single-molecule techniques. His current research deals with mechanistic questions of membrane transport proteins in bacteria, (bio)chemical catalysis and probe development for fluorescence microscopy.

where Φ_D is the donor quantum yield in the absence of an acceptor, N is Avogadro's number, n is the refractive index of the intervening solution, and κ^2 is the orientation factor describing the orientation of the two dipoles with respect to each other. The orientation factor is often a matter of debate and can only be set to $\kappa^2 = 2/3$ for the special case of unrestricted rotational freedom of at least one of the fluorophores.[16,17] The overlap integral is a function of the wavelength λ and is calculated using ε_A as the molecular extinction coefficient of the acceptor and f_D as the wavelength-dependent emission spectrum of the donor.[18]

The definition of FRET given above is not limited to single-molecule studies but rather includes ensemble-based studies. By using the term smFRET, however, we are specifically referring to techniques that measure FRET on a molecule-by-molecule basis. This approach allows us to look beyond the dynamic and static heterogeneity that may be present in complex (biological) samples but is often averaged out in standard bulk assays.

To experimentally realize smFRET, it is crucial to obtain a sufficiently high signal-to-noise ratio (SNR) to detect a single fluorescent molecule against the background created by a vast excess of solute molecules. Even though the first detection of smFRET was reported using a near-field scanning optical microscope,[11] the simplicity and high SNR of either confocal microscopy[19,20] or total internal reflection fluorescence (TIRF) microscopy[1,21,22] has allowed smFRET to flourish.[9,23–26]

In diffusion-based confocal microscopy, which is a major focus of this review, a femto-litre-sized excitation volume is created by focusing laser light with an objective of high numerical aperture into a sample containing a low, typically picomolar, concentration of fluorescently labelled and freely diffusing species (Fig. 1A). A combination of epi-fluorescence, *i.e.*, excitation and detection *via* the same objective, with a micrometer-sized pinhole creates a diffraction-limited detection volume around the excitation focus where the background signal is efficiently suppressed. After the pinhole, the fluorescence is divided into a donor and an acceptor detection channel using suitable spectral filtering (*e.g.*, bandpass filters) adapted to the properties of the donor and acceptor fluorophores. Each transit of a labelled molecule through the confocal volume will lead to the detection of a fluorescent burst as depicted in Fig. 1B and C. This allows determining the photon counts in a given detection channel. By recording the arrival time for each single photon, we can identify fluorescent "bursts" related to a molecular transit. Identification of this burst is done *via* a threshold criterion that detects the number of photons in a given time window, which is normally shorter than the mean diffusion time of the fluorescent species through the confocal volume.[27,28] Throughout this manuscript, we will continue to use this picture of bursts for all our considerations. We should emphasize, however, that all of the following relations and equations are also applicable for cases where, instead of using bursts, we measure a certain number of photons in a given time interval (binning). This approach represents a common strategy for surface-based confocal scanning microscopy and especially TIRF microscopy (Fig. 1D–F), in which single arrival times of photons are currently not accessible

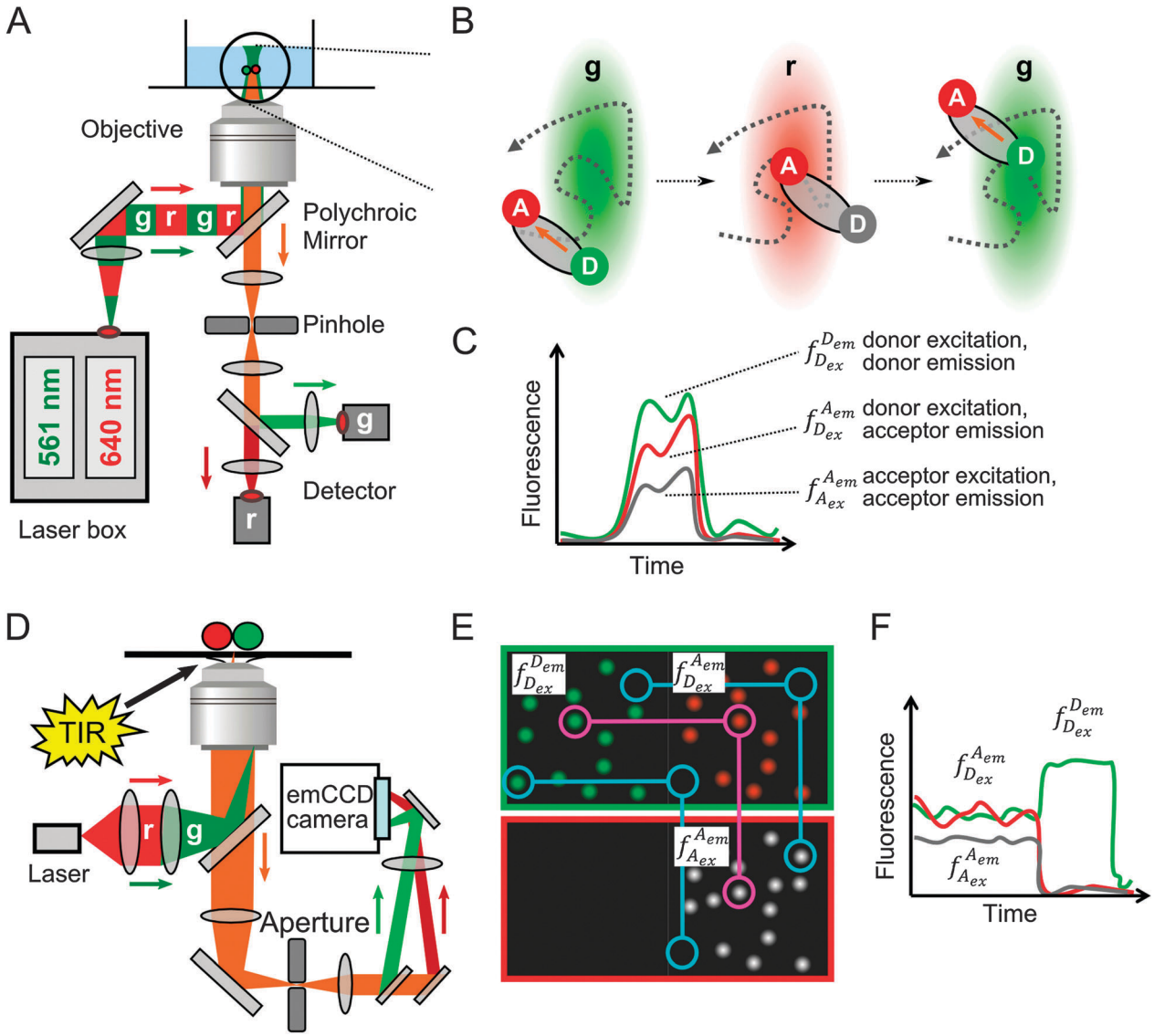

Fig. 1 Implementation of the alternating-laser excitation scheme in confocal and TIRF microscopy. (A) Confocal microscopy. The laser box in the excitation pathway contains two modulatable lasers in order to provide well-defined sequences of red (r) and green (g) illumination. After collimating the laser light with a lens and reflecting the laser by a polychroic mirror, an objective with high numerical aperture is used to generate a diffraction limited excitation spot in the sample volume. Fluorescence, originating from fluorescent dyes attached to biomolecules diffusing through the confocal spot, is collected by the same objective and spatially filtered with a pinhole before it is spectrally split into a green and a red detection channel. (B) During the transit of a single biomolecule through the focus, the periods of green (g) and red (r) excitation alternate much faster than the corresponding diffusion time. Upon direct excitation of the donor, some energy can be transferred to the acceptor *via* FRET. The existence of the acceptor is probed during red excitation. (C) As a result, every burst is characterised by three photon numbers: First, the number of photons in the donor channel after donor excitation $\left(f_{\mathrm{Dex}}^{\mathrm{Dem}}\right)$; second, the number of photons in the acceptor channel after donor excitation $\left(f_{\mathrm{Dex}}^{\mathrm{Aem}}\right)$; and third, the number of photons in the acceptor channel after direct acceptor excitation $\left(f_{\mathrm{Aex}}^{\mathrm{Aem}}\right)$. (D) TIRF microscopy. In contrast to a confocal microscope, the laser light is focused onto the backfocal plane of the objective, the image is spatially filtered with a rectangular aperture, and both detection channels (for donor and acceptor) are imaged onto a camera. (E) Schematic frames after donor excitation (top, green) and direct acceptor excitation (bottom, red). Individual particles are linked across the field of view and individual point spread functions (PSF) are fit to Gaussian distributions yielding positions of single species; the fluorescence intensity at these positions on the camera over time gives fluorescent time traces (F).

(for a review on recent developments in camera-based, fluorescence-lifetime-resolved imaging, see ref. 29).

Photon counts derived from time-binning or burst searches are then used to determine FRET efficiencies according to established methods from ensemble-based studies.[30,31] For smFRET the two important ones are (i) the calculation *via* "FRET-sensitized" emission by comparing the measured fluorescence intensities in the donor and the acceptor channel after donor excitation $f_{\mathrm{D_{ex}}}^{\mathrm{D_{em}}}$ and $f_{\mathrm{D_{ex}}}^{\mathrm{A_{em}}}$, respectively, and (ii) by using the decrease in the fluorescence lifetime of the donor in the presence of an acceptor (see eqn (1)). Here, we will focus on the first option, which does not require expensive instrumentation to measure fluorescence lifetimes.

For extensive reviews on smFRET and different experimental realizations, we refer the reader to ref. 2, 9, 23, 25 and 32.

smFRET and alternating-laser excitation (ALEX)

For each burst, we calculate apparent FRET E^*, which is used to reveal relative distance changes rather than exact distances as the photon counts are not yet corrected for background, spectral cross-talk of the donor into the acceptor-emission channel and detection efficiencies of the dyes (see section 'ALEX for accurate smFRET')

$$E^* = f_{D_{ex}}^{A_{em}} \Big/ \left(f_{D_{ex}}^{D_{em}} + f_{D_{ex}}^{A_{em}}\right). \quad (3)$$

Spectral cross-talk is a major problem in standard smFRET experiments that use only a single laser for excitation of the donor and rely on recording the emission from both donor and acceptor to calculate the FRET efficiency. This is because the emission spectrum of donor fluorophores is often so broad that some of the emitted donor photons are actually detected in the acceptor-emission channel. This has the severe consequence that the attribution of calculated transfer efficiencies to particular species is sometimes impossible, *e.g.*, in case of an indistinguishable convolution of donor-only and low-FRET species. Alternating-laser excitation (ALEX) solves this problem. This excitation scheme uses direct excitation of the donor fluorophore that is alternated with direct excitation of the acceptor fluorophore (see Fig. 1 and ref. 10 and 33–35). For diffusion-based confocal microscopy, in which the diffusion time of the fluorescent species is in the lower millisecond range, an alternation frequency of around 20 kHz is sufficient to directly excite the donor and the acceptor several times during the passage of a doubly labelled molecule through the confocal volume (Fig. 1B). In TIRF or confocal scanning microscopy lower alternation frequencies are used that are typically found in the millisecond time range.

Using the ALEX scheme, we gain access to an additional photon number for each burst $f_{A_{ex}}^{A_{em}}$, which represents the fluorescence detected in the acceptor-emission channel after direct excitation of the acceptor. (A fourth existing photon stream $f_{A_{ex}}^{D_{em}}$ is ignored as it does not contain a significant number of photons.) The three photon streams provide a way of verifying the presence of the acceptor in a fluorescently active form. Moreover, by defining the raw stoichiometry, we can relate the total fluorescence recorded after donor excitation to the total fluorescence after direct donor and acceptor excitation[34]

$$S^{raw} = \left(f_{D_{ex}}^{D_{em}} + f_{D_{ex}}^{A_{em}}\right) \Big/ \left(f_{D_{ex}}^{D_{em}} + f_{D_{ex}}^{A_{em}} + f_{A_{ex}}^{A_{em}}\right). \quad (4)$$

To understand the meaning of stoichiometry, it can be helpful to think of E^* and S^{raw} in terms of chromaticity: whereas E^* represents the detected chromaticity after excitation of the donor, which shifts to longer wavelengths (*e.g.*, red) with increasing FRET efficiency, S^{raw} represents the chromaticity after exciting both donor and acceptor (Fig. 2A). For a donor-only species, the chromaticity of S^{raw} is determined mainly by the excitation of

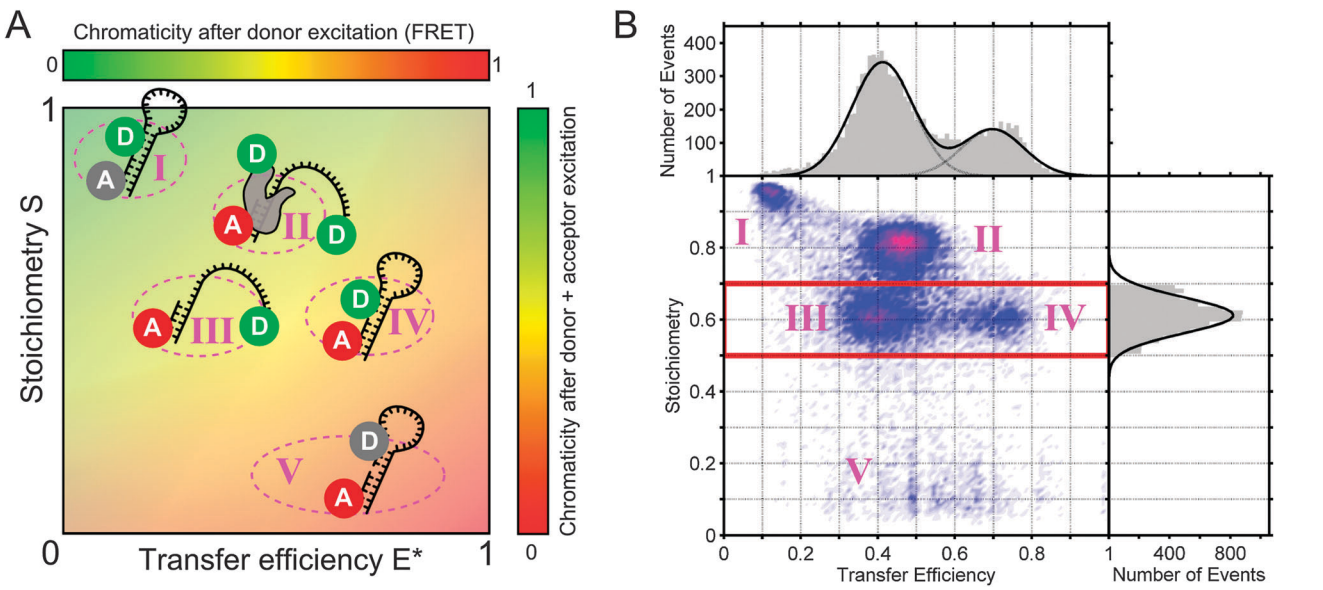

Fig. 2 Fluorescence-aided sorting using alternating-laser excitation. (A) Conventional single-colour laser excitation solely reports on the transfer efficiency E^*, which is here shown as the detected chromaticity after donor excitation representing the range from low-FRET species on the left to high-FRET species on the right. Using the alternating-laser excitation scheme, the stoichiometry S allows one to separate species based on their chromaticity after direct excitation of the donor and the acceptor: a donor-only sample (I), here shown as a doubly labelled DNA hairpin with a bleached acceptor, will show a high S value, whereas a acceptor-only sample (V) will appear with low S. Molecules bearing, for example, one acceptor and at least one donor dye will show an intermediate stoichiometry (II–IV). A two-dimensional *ES* histogram is generated by plotting the transfer efficiency *versus* the stoichiometry for each single burst (confocal detection) or for each molecule (camera-based detection). (B) Simulated data of five different species diffusing through a confocal volume using solution-based ALEX. The parameters used for the simulation were adjusted to mimic experimental conditions as closely as possible. Whereas the two-dimensional *ES* histogram allows differentiating all species unambiguously, the one-dimensional histogram of the transfer efficiency after single-colour excitation would have been too convoluted to separate species II and III. The one-dimensional bar histograms represent the data as defined by the red box.

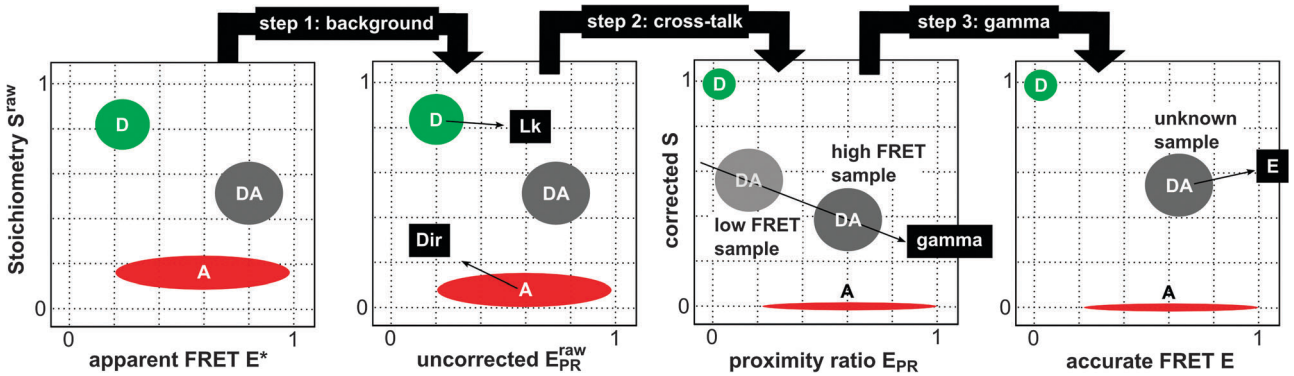

Fig. 3 Three steps towards accurate FRET. In the first step, the background intensity is subtracted from the detected photon streams. In the second step, the position of the donor-only and acceptor-only FRET species in the *ES* histogram allows determining the contributions of the leakage from the donor into the acceptor detection channel (Lk) and the direct excitation of the acceptor upon donor excitation (Dir). In the third step, the slope between the peaks of a low-FRET and a high-FRET species is fitted to determine the correction factor gamma. Note that applying each correction factor leads to a shift of the positions of each species in the *ES* histogram. After all corrections *E* can be determined from the DA population using, *e.g.*, Gaussian fitting. This accurate FRET value is then used to determine intramolecular distances with the knowledge of the Förster radius according to eqn (14).

the donor and $S^{raw} \sim 1$ (as $f_{A_{ex}}^{A_{em}} \sim 0$). For acceptor-only species, the chromaticity is therefore given by the colour of acceptor excitation and $S^{raw} \sim 0$ (as $f_{D_{ex}}^{A_{em}} + f_{D_{ex}}^{D_{em}} \sim 0$). The crucial point is now to tune the relative laser intensities for direct-donor and direct-acceptor excitation in such a way that species bearing both fluorophores exhibit a stoichiometry that is clearly distinguishable from the donor-only and acceptor-only species. In summary, knowledge of S^{raw} allows us to determine the labelling stoichiometry of the fluorescent species (Fig. 2A). By calculating both a FRET value and a stoichiometry value for each burst, we can plot the data in a two-dimensional *ES* histogram, which enables us to separate low FRET species from donor-only species based on their respective stoichiometry, thus extending the usable FRET range to very low values.

Having the stoichiometry as an additional parameter for sorting FRET data, one can increase the complexity of the samples[12] as is briefly demonstrated in a simulation of five fluorescent species freely diffusing in solution (Fig. 2B). Whereas species III and IV represent a donor–acceptor labelled molecule interconverting between two FRET states, a new independent species (II) with a higher stoichiometry can be identified. This second donor molecule shifts the chromaticity of the stoichiometry towards the colour of the donor excitation. It should be noted that this additional species would have severely complicated the analysis of a FRET histogram taken after single-laser excitation.

So far, we required the frequency of alternation to be faster than the related diffusion time of a molecule through the focus (20 kHz *versus* 1 ms), but several publications suggest the use of pulsed lasers to modulate the alternation in the nanosecond range (nsALEX/PIE) as we will discuss below.[36,37] However, slow alternation frequencies provide a convenient way to determine molecular distances from histograms of transfer efficiencies with affordable and simple experimental setups.

ALEX for accurate smFRET

ALEX-based smFRET detection allows sorting species based on their FRET efficiency and their (labelling) stoichiometry. However, even if we can identify various species using the two-dimensional *ES* histogram, we still face the challenge of translating transfer efficiencies into molecular distances. The major obstacles that we have to overcome are (1) the background intensity contributing to all three photon streams $f_{D_{ex}}^{A_{em}}$, $f_{D_{ex}}^{D_{em}}$, and $f_{A_{ex}}^{A_{em}}$, arising from impurities, inelastic Raman scattering of the water molecules, and dark counts in the detectors, (2) the two cross-talk terms, (i) the leakage Lk of the donor-emission into the acceptor-detection channel and (ii) the direct excitation Dir of the acceptor fluorophore by the laser used for exciting the donor, and (3) the overall photon-detection efficiencies in the detection channels (represented by γ). A detailed discussion of accurate FRET is given by Lee *et al.*[34]

Here, we present a concise method for the sequential determination and application of all the correction parameters needed for measuring accurate FRET distances using ALEX-spectroscopy (Fig. 3). With a typical sample, the cross-talk correction terms are determined from the same data as would normally be collected for standard analysis, *i.e.*, distance measurements in a sample, while gamma can be determined by the comparison of two or more such data sets on constructs with different FRET efficiencies.

Correction 1: background

The background intensities (counts per unit time) in confocal microscopy can be estimated either by determining the count rate between bursts or by calculating the mean count rate in each channel. The latter method is often sufficiently accurate, given that the concentration of fluorescent molecules in solution is below 100 pM – a requirement which is already met in order to observe single molecules in the confocal volume. Thus for each burst, the background-corrected photon counts ${}_c f_j^i$ for the three photon streams are calculated by subtracting the background count rate (for each stream) multiplied by the length of the burst.

In accordance with the above considerations we calculate the proximity ratio E_{PR}^{raw}, which is not yet corrected for spectral cross-talk

$$E_{PR}^{raw} = {}_{c}f_{D_{ex}}^{A_{em}} \Big/ \left({}_{c}f_{D_{ex}}^{D_{em}} + {}_{c}f_{D_{ex}}^{A_{em}}\right). \quad (5)$$

Correction 2: cross-talk

In the presence of both donor and acceptor dyes and the possibility of FRET occurring between them, there are up to three contributions to the donor-excitation acceptor-emission photon stream

$${}_{c}f_{D_{ex}}^{A_{em}} = \mathrm{Lk} + \mathrm{Dir} + F^{\mathrm{FRET}}. \quad (6)$$

Lk and Dir were defined above and F^{FRET} represents the number of photons arising from acceptor emission after energy transfer from the donor fluorophore. By selecting donor-only or acceptor-only populations from a background-corrected *ES* histogram (populations I and V, respectively, in Fig. 2A), it is possible to determine the contributions from Lk and Dir to the ${}_{c}f_{D_{ex}}^{A_{em}}$ photon stream and thus calculate F^{FRET} for each individual burst.

The donor-only species, which may be present in our sample due to incomplete labelling or acceptor photobleaching, gives direct access to the leakage contribution. We obtain ${}_{c}f_{D_{ex}}^{A_{em}} = \mathrm{Lk}$ as there can be no photons arising from either direct excitation of the acceptor (Dir = 0) or FRET ($F^{\mathrm{FRET}} = 0$). As the leakage Lk is proportional to the total number of donor photons detected in the donor channel, we write $\mathrm{Lk} = l \cdot {}_{c}f_{D_{ex}}^{D_{em}}$ and thus ${}_{c}f_{D_{ex}}^{A_{em}} = l \cdot {}_{c}f_{D_{ex}}^{D_{em}}$ for donor-only molecules using l as the leakage coefficient. Continuing with donor-only molecules, we find that eqn (5) now simply reads $E_{\text{D-only}} = l/(l + 1)$, which represents the peak of the apparent transfer efficiencies of the donor-only molecules and is therefore used to determine the leakage coefficient

$$l = E_{\text{D-only}}/(1 - E_{\text{D-only}}). \quad (7)$$

Applying a similar line of reasoning to acceptor-only molecules yields ${}_{c}f_{D_{ex}}^{A_{em}} = \mathrm{Dir}$. We can use the direct-excitation coefficient d to define $\mathrm{Dir} = d \cdot {}_{c}f_{A_{ex}}^{A_{em}}$ and thus ${}_{c}f_{D_{ex}}^{A_{em}} = d \cdot {}_{c}f_{A_{ex}}^{A_{em}}$. Substituting into the equation for the stoichiometry (eqn (4), but using the background-corrected photon counts) gives $S_{\text{A-only}} = d/(d + 1)$ from which we calculate d as

$$d = S_{\text{A-only}}/(1 - S_{\text{A-only}}). \quad (8)$$

In summary, by fitting the peaks of the donor-only and acceptor-only species to obtain all correction factors, we calculate F^{FRET} for each individual burst

$$F^{\mathrm{FRET}} = {}_{c}f_{D_{ex}}^{A_{em}} - \mathrm{Lk} - \mathrm{Dir} = {}_{c}f_{D_{ex}}^{A_{em}} - l \cdot {}_{c}f_{D_{ex}}^{D_{em}} - d \cdot {}_{c}f_{A_{ex}}^{A_{em}}. \quad (9)$$

We can now calculate the cross-talk-corrected proximity ratio E_{PR}

$$E_{PR} = F^{\mathrm{FRET}} \Big/ \left({}_{c}f_{D_{ex}}^{D_{em}} + F^{\mathrm{FRET}}\right) \quad (10)$$

and the cross-talk-corrected stoichiometry S

$$S = \left({}_{c}f_{D_{ex}}^{D_{em}} + F^{\mathrm{FRET}}\right) \Big/ \left({}_{c}f_{D_{ex}}^{D_{em}} + F^{\mathrm{FRET}} + {}_{c}f_{A_{ex}}^{A_{em}}\right) \quad (11)$$

Correction 3: gamma

The last step towards fully corrected transfer efficiencies E is the determination of the correction factor γ, which itself represents the ratio of the quantum yields and the detection efficiencies of donor (without an acceptor nearby) and acceptor, respectively. A gamma factor of $\gamma \neq 1$ causes the stoichiometry of species with different FRET values also to be different. To determine γ we have to use (at least two) peak positions S_i and $E_{PR,i}$ of two FRET samples to plot $1/S_i$ *versus* $E_{PR,i}$. We obtain the intercept Ω and the slope Σ from a linear fit and we calculate γ according to

$$\gamma = (\Omega - 1)/(\Omega + \Sigma - 1). \quad (12)$$

With that information we can re-calculate E as

$$E = F^{\mathrm{FRET}} \Big/ \left(\gamma {}_{c}f_{D_{ex}}^{D_{em}} + F^{\mathrm{FRET}}\right) \quad (13)$$

and we gain access to the molecular distances with

$$R = R_0((1 - 1/E) - 1)^{1/6}. \quad (14)$$

The crucial parameter in converting accurate FRET efficiency to molecular distance is the Förster radius, R_0 (see eqn (2)). Because this parameter may be affected by the microenvironment of the fluorophores, it is advisable to determine the R_0 experimentally, rather than rely on theoretical values. The quantum yield of the donor dye can be determined using a donor-only labelled construct, by comparison to a dye with a known quantum yield.[38] Equally, the overlap integral (eqn (2)) can be calculated from the donor emission spectrum and the acceptor absorbance spectrum. However, the determination of the orientation factor is less straightforward. If the measured steady-state ensemble anisotropies of donor-only and acceptor-only species are low (0.1–0.25), thereby indicating rotational freedom of the dyes over the lifetime of the excited state, the assumption of $\kappa^2 = 2/3$ is reasonable and possible errors arising from this are generally small ($\sim$10%).[39] A more sophisticated approach takes account of the orientation factor by simulating possible values of R_0 based on the steady-state ensemble anisotropies of donor and acceptor dyes and the R_0 in the isotropic ($\kappa^2 = 2/3$) case.[40] Another alternative method uses the measured FRET efficiencies between donor and acceptor dyes attached to a rigid protein domain, in conjunction with the calculated fluorophore separation from the crystal structure, to calculate an empirical R_0.[41]

It should be noted that the correction process for accurate FRET described above can be applied directly to data from TIRF measurements, where the detected intensities from single molecules are imaged onto a camera (Fig. 1D–F). The intensity traces are obtained by fitting a two-dimensional Gaussian across the molecule and we obtain binned photon counts $\left(f_{D_{ex}}^{A_{em}}, f_{D_{ex}}^{D_{em}} \text{ and } f_{A_{ex}}^{A_{em}}\right)$ for each particle,[42] similar to confocal data. Interestingly, with TIRF data, it is actually possible to determine many of the correction parameters on a molecule-by-molecule basis. A comparison of the relative merits of this with other approaches to accurate FRET would be a useful next step in standardising these methods for wider use.

Applications of solution-based ALEX microscopy

The introduction of ALEX in 2004 enabled researchers to reconsider the design of smFRET-based assays. ALEX made it possible to utilise transfer efficiencies smaller than 0.4, without having to worry about potential convolutions of low-FRET and donor-only species. This created the possibility for the development of interesting biophysical assays to assess (static) protein structures and their working mechanisms using ALEX-type experiments, some of which are highlighted here. The examples include processes directly associated with the central dogma of molecular biology (transcription, replication) but also other vital processes such as molecular transport.

Bacterial transcription

In 2006, Kapanidis *et al.* used a variety of fluorescently labelled DNA constructs, partially in conjunction with a labelled sigma factor, bound to bacterial RNA polymerase (RNAP), to investigate the mechanism of transcription initiation complexes in RNA polymerases.[43] Transcription initiation is the first and most highly regulated process in gene expression, and several competing mechanisms had been discussed in the literature.[43–48] Using ALEX-spectroscopy, the authors found direct evidence for a "scrunching" mechanism, in which the polymerase remains fixed on promoter DNA and downstream DNA is pulled into the polymerase itself. The mechanism was supported by another study where bubble formation was observed directly. It was detected using quenchable FRET in which closely spaced fluorophores acting as the donor and the acceptor quench each other until RNA polymerase opens the DNA thereby unquenching both fluorophores.[49]

The group also demonstrated conformational dynamics within the catalytically active RNAP–DNA open complex with ALEX.[50] This study provided the first direct observation of conformational dynamics in the transcription bubble of the open complex. These results also led to the important conclusions that the mechanism of active search for transcription start sites provides an alternative route for gene regulation.[50]

ALEX-based smFRET was also used to show directly opening and closing of the RNA polymerase clamp at each step in transcription initiation and elongation[51] (Fig. 4A). The figure shows 2-colour ALEX data of the RNAP holoenzyme (RNAP and transcription factor σ^{70}) in solution which adopts multiple conformational states: open (E = 0.15, 8.1 nm), closed (E = 0.28, 6.9 nm) and collapsed (E = 0.40, 6.4 nm) with a predominant occurrence of the open state (>50%). The same behaviour was found for the core enzyme (RNAP) rendering this mix of conformations as an intrinsic property of the core rather than the holoenzyme. Upon addition of DNA, the closed state is populated with 100% (E = 0.31, 6.9 nm). No further changes are observed for addition of nucleoside triphosphate subsets: Both the initial transcribing complex with nascent RNA (RPitc, 4–7 nt of RNA) and early elongation complexes (RDe, 14 nt of RNA) show similar FRET distributions indicating that no change in the clamp structure occurs upon scrunching and promoter escape.

This work required the labelling of different sites using unnatural amino acids.[52–54] Conventionally, proteins are fluorescently labelled using maleimide dyes reacting with naturally occurring or, more often, artificially introduced cysteines. However, as many enzymes have conserved cysteines, labelling strategies using cysteines are often limited and new strategies have to be employed.

Identifying dynamics

So far, the presented analysis of FRET distributions only made use of their mean values, which are at least for static FRET species straightforward to obtain and to interpret. However, the situation is more complicated for mixtures of multiple, static FRET species or species interconverting between multiple FRET states. Therefore, several groups started developing a statistical framework, with the aim of analysing the width and the overall shape of FRET distributions.[28,55–59] These approaches can be summarised as Probability Distribution Analysis (PDA) methods, as they aim at recapitulating FRET distributions based on the experimentally obtained distributions of photon counts. These PDA based methods can also be used to determine the number of subspecies and eventually disentangle them.[60]

In the context of applying ALEX, Nir *et al.* presented an algorithm for the calculation of a shot-noise limited proximity ratio histogram.[28] The publication also introduced a variety of different methods for ALEX-based burst detection and demonstrated how effects like fluorophore bleaching and blinking (see also ref. 61 for a discussion of photobleaching pathways), the coincident events of different species diffusing simultaneously through the focus, and detection volumina mismatches can be identified in a *ES* histogram. The paper proved to be essential for the development of Burst Variance Analysis (BVA)[62] and dynamic Probability Distribution Analysis (dPDA),[63] two methods which allow the identification and characterisation of dynamic changes in the transfer efficiency. In BVA, the transfer efficiency is calculated for every five photons detected after excitation of the donor.[62] Every single burst will contain many of these five-photon windows and the standard deviation calculated over all windows of one burst will indicate whether the system is likely to be dynamic beyond the value expected for a pure shot-noise based photon distribution in one of the two channels for donor or acceptor detection, respectively. Similar approaches have been described elsewhere.[60,64] Dynamic PDA on the other hand calculates how a histogram of transfer efficiencies would look for a species interconverting between two FRET states.[63] Comparison of the simulated histograms to experimental data allows the determination of the rates by which the dynamic systems change their conformation.

DNA repair

Both BVA and dynamic PDA were applied to characterise the conformational dynamics of the bacterial DNA polymerase I (Klenow fragment, KF).[63,65,66] The work on KF was initiated by the existence of two crystal structures; the first showed the binary complex formed by DNA and the enzyme in an open

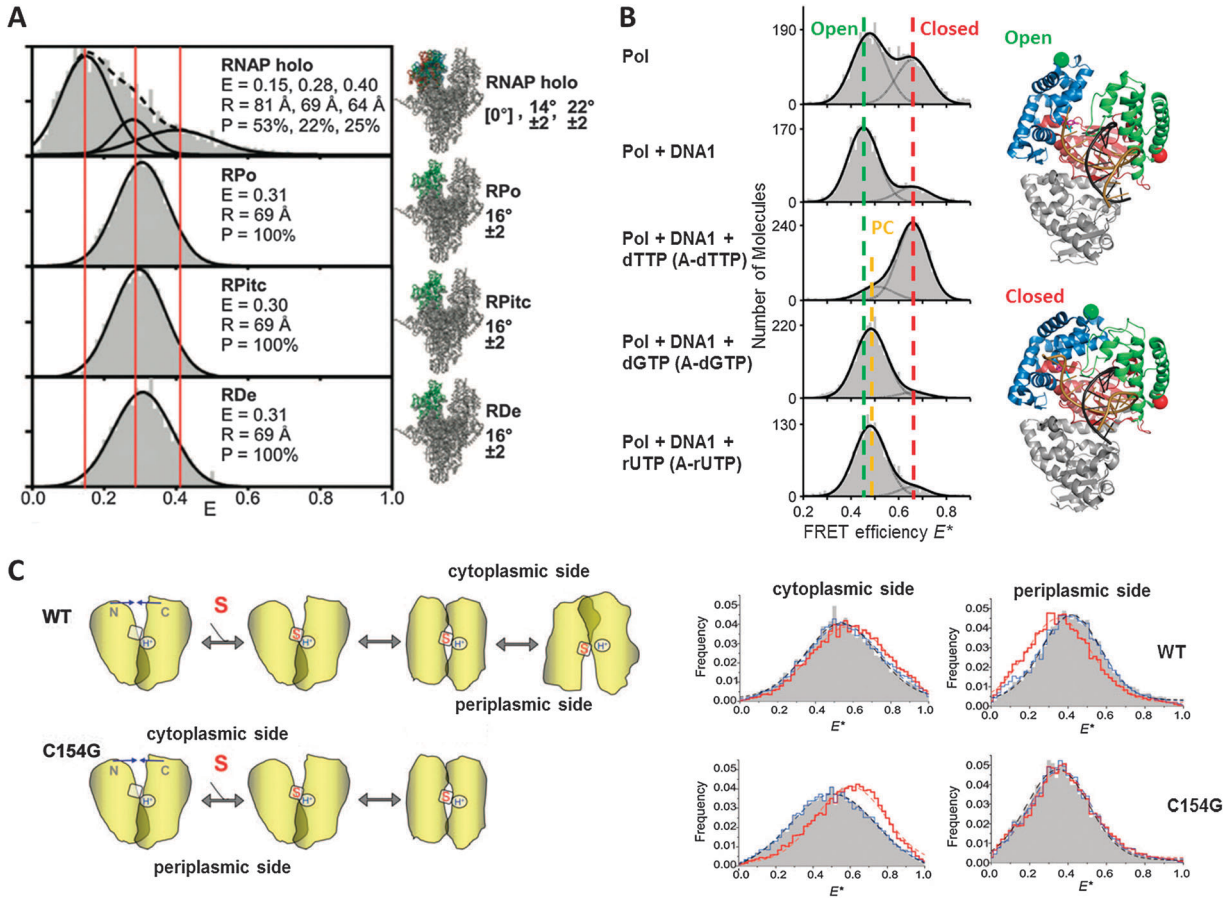

Fig. 4 Biophysical applications of ALEX-based smFRET. (A) ALEX-based study of the RNAP clamp conformation in σ^{70}-dependent transcription initiation and elongation (adapted from ref. 51 and reprinted with permission from AAAS). Histograms and Gaussian fits show observed accurate FRET values *E* (at left) with mean *E*, mean distance between probes *R*, and percentage *P* for each subpopulation. The inferred structural states of the RNAP clamp and the extent of closure are indicated next to the structure on the right. See the main text for more details. (B) Conformational landscapes of DNA polymerase 1 (Klenow fragment) (adapted from ref. 66). The unliganded enzymes show a dynamic equilibrium between an open and a closed conformation of the fingers subdomain (shown in blue in the crystal structures based on ref. 67). Addition of DNA (with A as the templating base) shifts the equilibrium towards the open state. The ternary complex with correct nucleotides (1 mM dTTP) shows most molecules in the closed conformation, whereas the ternary complex formed with incorrect nucleotides (1 mM rUTP or 1 mM dGTP) adopts a partially closed conformation. Nucleotide titrations were used to verify the subtle peak shifts from the open to the partially closed conformation.[66] (C) Cartoon model of conformational changes in LacY detected by smFRET/ALEX including experimental data supporting the model for wild-type (wt) and C154G mutant (adapted from ref. 70, copyright (2007) National Academy of Sciences, U.S.A.). See the main text for more details.

conformation, and the second showed the ternary complex formed by DNA, a complementary nucleotide and the enzyme in a closed conformation.[67] After labelling the thumb subdomain with an acceptor and the fingers subdomain with a donor fluorophore, the authors could identify both open and closed conformations (Fig. 4B). The smFRET assay also revealed the previously unknown existence of an intermediate FRET state,[65] which was later identified and further characterised as a partially closed state of the polymerase which is an essential fidelity checkpoint of the polymerase.[66,68] Even though the smFRET assay used a rather conventional range for the transfer efficiencies (>0.4), ALEX helped to build confidence in the data given that the change in the inter-fluorophore distance between the open and the partially closed conformation is only around 0.2 nm. Another important result of these studies was the observation that the unliganded polymerase populated both the open and the closed conformations, interconverting between them on the single-digit millisecond time scale, thereby demonstrating the high degree of conformational flexibility in the absence of any ligand.[65,66]

The feature of unliganded enzymes populating conformational states along the reaction pathway has also been demonstrated for *Aquifex* adenylate kinase using a smFRET assay in which the lids for AMP and ATP were fluorescently labelled.[69]

Membrane transport

Membrane proteins are key players in all three kingdoms of life and are involved in nearly every cellular process. They regulate ion gradients, facilitate energy conversion, control cell properties and more generally orchestrate molecular transport. Despite their importance, numerous questions about the working mechanism are unclear, including conformational states and

protein stoichiometry that occur during transport and the central question of how energy utilization (ATP-hydrolysis, co-transport of ions) is coupled to conformational changes that drive transport.

A model system was recently investigated using ALEX-spectroscopy, *i.e.*, lactose permease (LacY) of *E. coli.*[70] It actively drives the transport of galactopyranosides using an electrochemical gradient of protons in a symport mechanism. It was hypothesized that an outward-facing cavity opens during symport with simultaneous closing of the inward-facing cavity so that the sugar-binding site is alternately accessible to either face of the membrane. The authors used ALEX spectroscopy to study the conformational states of this transporter and to characterize ligand-induced changes in the cytoplasmic and periplasmic sides in detergent. In the absence of a ligand (sugar, S) the protein is in a protonated state with an inward-facing hydrophilic cavity. This gives rise to intermediate apparent FRET E^* of $\sim$0.5 (see gray FRET distributions from ALEX measurements on the right side of Fig. 4C). Without a ligand, both proteins (wt, C154G) have multiple conformations on the cytoplasmic side as well as the periplasmic side (arrows). Binding of a ligand (4-nitrophenyl-α-D-galactopyranoside, NPG) induces a global conformational change in both wild-type LacY and the C154G mutant resulting in closing of the inward-facing hydrophilic cavity (see the cartoon model and red E^*-distribution with increased mean E^* for wt/C154G on the cytoplasmic side). A cavity opens on the periplasmic side in wild-type LacY allowing the substrate to be released (see red decreased E^*-distribution with decreased mean E^* for wt), and conformational heterogeneity increases after sugar binding. In contrast, the periplasmic cavity in the C154G mutant does not form easily after sugar binding, corresponding to a reduced number of conformers in the ligand bound state and restricted access for the sugar from the periplasmic side (see unchanged red E^* distribution for the periplasmic side for sugar addition). Control experiments with a non-binding sugar (4-nitrophenyl-α-D-glucopyranoside, NPGlc) support the interpretations of ligand-induced FRET changes.

These results provide strong evidence that wild-type LacY, bound to galactopyranoside, but not to glucopyranoside, has a decreased distance on the cytoplasmic side and an increased distance on the periplasmic side (Fig. 4C). In a mutant protein, a more pronounced decrease in distance is observed on the cytoplasmic side with no accompanying change on the periplasmic side. The results are fully consistent with the widely accepted alternating access model.

Technical advances of ALEX and resulting possibilities

To validate the broad applicability of solution-based ALEX we briefly mention the following examples where reversible conformational changes of DNA nanostructures,[71] the magnesium dependent conformational equilibrium of the human mitochondrial lysine transfer RNA,[72] the DNA unwrapping in nucleosomes,[73] and the structural dynamics of an autonomous bipedal DNA motor[74] were monitored. In this section we show how ALEX was advanced from a technical viewpoint to allow easier data acquisition or to get more information about the system of interest.

The diffusion-based part of the work on *Aquifex* adenylate kinase[69] used a variation of ALEX in which a laser operating in a continuous-wave mode for donor excitation is used in conjunction with a pulsed laser for direct excitation of the acceptor. The photons after red excitation are then identified and filtered with a setup suitable for measuring fluorescence lifetimes as the majority of photons will be detected within a few nanoseconds after the red laser pulse. This technique is also known as periodic acceptor excitation spectroscopy.[75]

If both lasers are being modulated in the nanosecond range, we refer to it as nsALEX[36] or Pulsed Interleaved Excitation (PIE).[37] Especially the use of two pulsed lasers offers intriguing new possibilities. First, the transfer efficiencies for the different species can be calculated using their fluorescence lifetimes. Second, as the alternation is now several orders of magnitude faster than the corresponding diffusion time of the species through the focus, the calculation of auto- and cross-correlation functions within and between the different detection channels is not affected as in the case of slow alternation speeds and can be used to determine diffusion coefficients and interactions between donor and acceptor labelled species.[37,76,77] For example, a setup capable of PIE has been used to study the conformational dynamics of chaperones[78] and by combining PIE with the multi-parameter fluorescence detection (MFD) scheme, introduced by the Seidel group a decade ago,[79,80] a solid framework for diffusion-based confocal experiments has been established as recently summarised.[32,81] For pulsed-interleaved excitation, supercontinuum lasers have been employed to provide a convenient and relatively affordable way of exciting fluorophores at user-selectable wavelengths.[82]

So far, we have discussed ALEX between a donor and an acceptor fluorophore. A number of authors, however, suggest the use of more fluorophores to measure multiple distances and interactions at the same time. Three-colour ALEX[83] and even four-colour ALEX[84,85] (Fig. 5A) have been demonstrated for diffusion-based confocal microscopy, but the complexity of data analysis and the demanding requirements on the labelling efficiencies for each component increase the experimental complexity tremendously and limit the range of possible applications.

Interestingly though, this highlights one of the drawbacks of confocal microscopy which is the limited throughput achievable with this technique. To avoid the case of having two non-interacting species in the confocal focus, the concentration of the fluorescent species has to be kept very low (pM range). Before we continue discussing camera-based approaches in the next sub-section, one publication should be mentioned which reported on the combination of a confocal microscope with a microfluidic-based device for titration experiments.[86] Here, the RNAP activity of transcribing poly(dA) was measured as a function of potassium glutamate concentration by hybridising a doubly labelled poly(dT) probe, which decreased its transfer efficiency upon forming a double-stranded RNA. The key aspect of the work is to provide a turnkey solution, in which

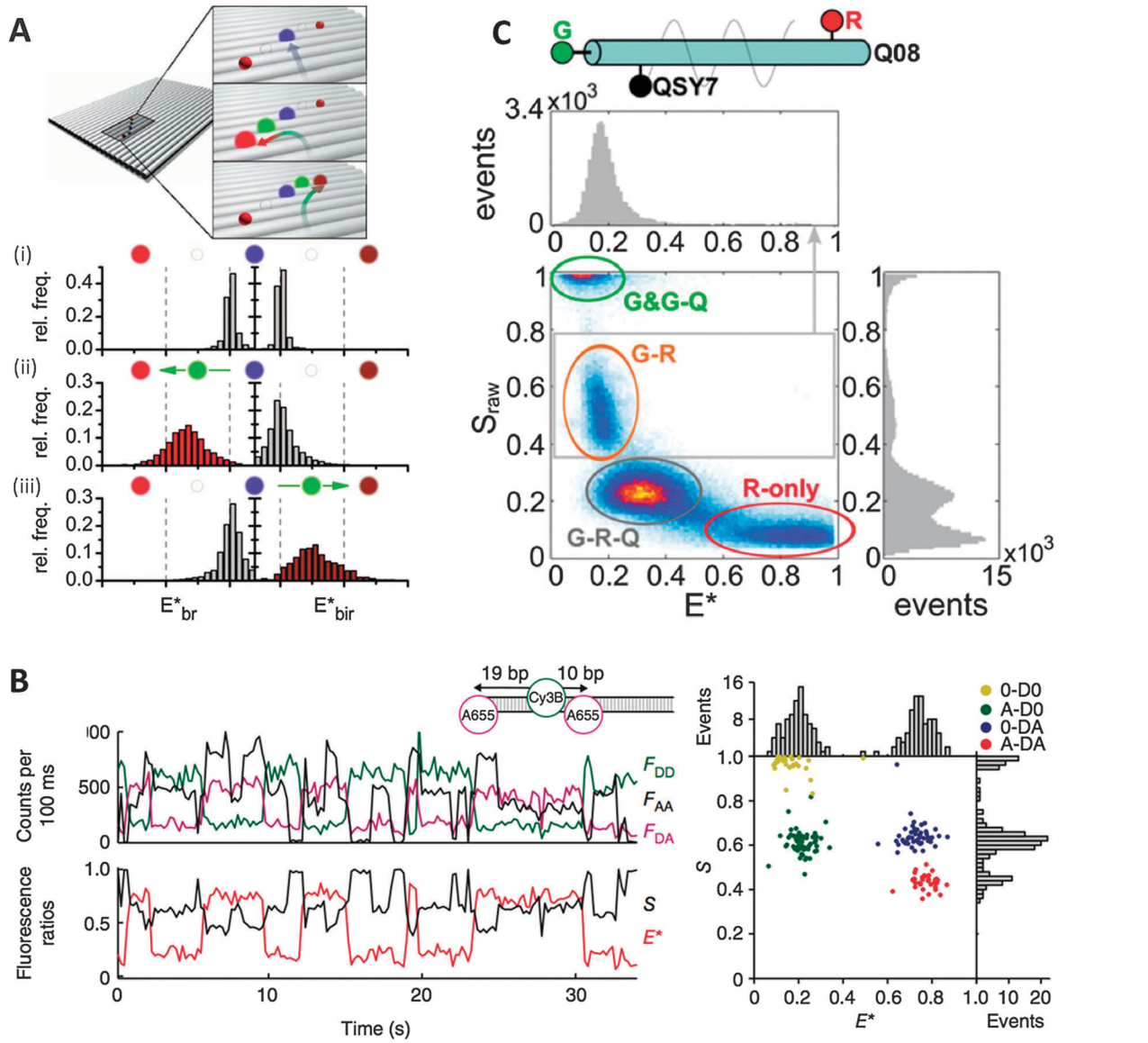

Fig. 5 Technical advances in ALEX-spectroscopy. (A) The top part shows the arrangement of fluorophores on a rectangular DNA origami and visualization of alternative energy-transfer pathways with a ''jumper'' dye guiding the light from the blue input to either the red or the IR output (reprinted with permission from ref. 85, American Chemical Society, copyright 2011). The other panels show the corresponding data from 4-colour ALEX measurements for the following scenarios: (i) co-localization between the donor (blue) and the two final acceptors (red and near-infrared) but no energy transfer indicated by E_{br}* = 0 and E_{bir}* = 0; (ii) directed energy transfer ''to the left'' by inserting a green transmitter increasing E_{br}* to 0.34 and (iii) directed energy transfer ''to the right'' by inserting a green transmitter (''jumper'') increasing E_{bir}* to 0.25. (B) Switchable FRET with two acceptors (reprinted with permission from ref. 103, Macmillan Publishers Ltd, copyright 2010). DNA molecules labeled with a single donor and two acceptors are immobilised on a glass surface. The chemically induced blinking of the individual acceptors can be monitored *via* direct excitation and the corresponding fluorescence ratios *E** and *S* allow resolving the individual contributions in an *ES* histogram. (C) Dark quencher chromophores as nonfluorescent acceptors (reprinted from ref. 105 with permission from Biophysical Society, copyright 2012). The DNA was labelled with a donor –G– and two acceptors, one of which was fluorescent –R– and the other one a dark quencher –Q–. Depending on the position of the dark quencher between the two fluorophores, the *ES* histogram is modulated which effectively allows determining the proximity of the quencher to either fluorophore. Note that for modulation of the stoichiometry by the G–R–Q species, FRET between the fluorophores is not required.

multi-dimensional (*e.g.*, salt-) dependencies can be investigated with a minimum of hands-on time and the highest possible mixing accuracy.

Up to this point, we have considered ALEX as an extension of smFRET. In the limit of FRET values close to zero, however, the stoichiometry becomes a reporter of coincidence between a donor labelled and an acceptor labelled entity in an, often diffraction limited, excitation and detection volume similar to coincidence spectroscopy.[87–89] This is especially interesting for the development of biosensors, which do not necessarily require energy transfer between donor and acceptor fluorophores for their successful implementation.[12,35] Lymperopoulos *et al.*

showed by a change in stoichiometry that transcription factors stabilise the binding of two double-stranded DNA fragments containing fluorescently labelled single-stranded complementary overhangs without significant FRET between the donor and the acceptor.[12]

ALEX-based smFRET in imaging-based microscopy

A major limitation of solution-based approaches, including ALEX-spectroscopy, is the limited observation time (<1 ms) dictated by the duration of diffusion through the confocal volume. In contrast, imaging-based microscopy such as TIRF and wide field microscopy allows monitoring hundreds and even thousands of single fluorescent, surface-immobilized molecules in parallel,[90] while also giving access to the history of each molecule for an extended period of time. Inevitably, ALEX was quickly adapted for TIRF and the first publication in 2006 demonstrated the abortive initiation and promoter escape of RNA transcription complexes.[91] Of utmost importance for surface-based single-molecule detection was the development of additives for oxygen scavenging and triplet quenching which nowadays allow the detection of millions of photons from single fluorescent emitters,[92,93] as recently reviewed in ref. 94. These developments enabled ALEX to be successfully expanded to multicolour excitation and detection schemes. Three-colour ALEX was demonstrated,[95] and extensions allow for up to four-colour FRET detection.[96–98] However, several methods were suggested to measure more than one distance quasi-simultaneously using a two-colour excitation and detection scheme. The first method, switchable FRET, uses the chemically induced stochastic blinking[99–101] of several acceptor fluorophores[102] on either a DNA (Fig. 5B) or a CAP binding protein to measure several distances from a single donor fluorophore to one of the particular acceptors which is currently in its active, non-dark state.[103,104]

The second technique uses a non-fluorescent dark quencher, which, depending on its distance relative to the donor and the acceptor fluorophore, modulates the detectable intensities of both fluorophores.[105–107] Note that in an ALEX scheme the quencher can modulate both the apparent FRET efficiency and the apparent stoichiometry[105] (Fig. 5C). A great advantage of using quencher-labelled enzymes is that they can be used in TIRF experiments at concentrations of 1 μM or more (compared to a maximum of ~100 nM for fluorophore-labelled species) without introducing a significant background, enabling the study of interactions of moderate-to-low affinity.

Holden *et al.* determined the achievable spatial and temporal resolution in ALEX-based smFRET experiments in TIRF microscopy by analysing the influence of major sources of noise.[42] The authors concluded that photophysics and focal drift are the main limiting factors for FRET resolution, but that single-basepair resolution is indeed obtainable at the single molecule level for short integration times (20 ms, 60 photons per ms per molecule).

In addition to using the direct acceptor excitation for accessing the stoichiometry and reporting on the photophysics of the acceptor fluorophore, a recent publication added the fitted width of the 2D Gaussian representing the acceptor emission after direct excitation as an additional parameter, which in that case reported on the diffusional freedom of the fluorophore attached to a long, surface-immobilised DNA molecule.[108] The experiment showed that after successful site-specific recombination of a Cre–loxP complex, an acceptor fluorophore, which was initially far away from a donor fluorophore, ended up closer to the donor fluorophore. This was concluded by monitoring the decrease in the width of the associated point spread function of the acceptor and the occurrence of FRET from the donor to the acceptor.

Imaging-based ALEX has been used further to study the translational dynamics of ribosomes[109–111] and the mechano-chemical cycle of the heat shock protein HSP90.[112]

ALEX: looking ahead

ALEX for structural biology

Single-molecule fluorescence techniques have traditionally focused on elucidating mechanistic details, with assays developed to monitor the kinetics and equilibria of many important processes, some of which are discussed above. However, recent efforts have extended the single-molecule toolkit for applications in structural biology.[113] While X-ray crystallography and NMR spectroscopy have been used to generate the bulk of high-resolution structures, large, multi-component, transient or dynamic complexes remain a challenge for these methods. Many of these difficulties can be overcome by single-molecule approaches, which remove ensemble averaging, and enable the detection and structural characterisation of various subspecies in dynamic equilibrium.

The general approach to defining a FRET-restrained structure involves the measurement of multiple pair-wise distances between donor and acceptor fluorophores, attached to specific sites on separate structural elements of a complex. These distances are then used as restraints for molecular modelling, in conjunction with any known structural information (*e.g.*, X-ray data for the individual structural elements), to produce a three-dimensional model, often using rigid body docking. A detailed discussion of these methods is presented in ref. 114.

Using this approach with ensemble FRET, Mekler *et al.* were able to define three-dimensional structures of the bacterial RNA polymerase (RNAP) holoenzyme and the RNAP-promoter open complex in solution.[115] Details of the eukaryotic RNA polymerase II elongation complex have also been elucidated using smFRET restraints derived from immobilised molecules.[116]

One of the challenges encountered with FRET-restrained structural determination is how to relate interdye distances to biomolecular structure. Because of the flexibility of the linker, the dyes populate a range of positions relative to their attachment points. Modelling these distributions is essential for the accuracy

of FRET as a quantitative structural tool. A popular method is to use molecular dynamics (MD) simulations to obtain the mean dye position, using an atomic model of the dye and linker attached to the specific atom in the biomolecule.[41,117–119] However, this approach is computationally expensive, so a simpler way to determine mean dye positions was developed by Muschielok *et al.* as a part of their probabilistic data analysis approach known as the nano-positioning system.[40,120] This method calculates the accessible volume (AV) of a dye (modelled as a sphere), attached to a specified atom by a flexible linker of certain effective length and width (Fig. 6A). A geometric search algorithm finds all dye positions within the linkage length from the attachment point, which do not cause steric clashes with the biomolecule. For dyes attached to DNA, the results from this approach were found to be consistent with those obtained by MD calculations. However, for more sterically demanding local environments, for example in RNA, Sindbert *et al.* found that it was important to perform three separate AV calculations, using three different radii to more accurately take into account the three quite different dimensions of the fluorophore.[121] Kalinin *et al.* combined this approach with a rigid body docking algorithm in their FRET positioning and screening software.[39] Measured donor–acceptor distances were modelled as springs with equilibrium length, R_{mp} and a strength (spring constant) derived from the corresponding measurement error (Fig. 6B). Using this method the authors produced a structure of the human immunodeficiency virus reverse transcriptase–DNA complex that agreed remarkably well with an X-ray structure of the same complex. This work provided a benchmark for the accuracy of FRET-derived structures, and confirmed smFRET as a useful tool for quantitative structural biology.

Interdye distances derived from the accurate FRET treatment of ALEX data (described above) can be used as restraints in the molecular modelling methods detailed here. ALEX is an attractive method for obtaining these distances, as it does not require expensive equipment or complicated analysis techniques. DNA–protein complexes are particularly promising targets for FRET-restrained structural determination. Multiple fluorophore positions can be introduced on DNA molecules with ease, thus reducing the need for extensive mutagenesis on the protein in order to obtain sufficient numbers of distance restraints.

In summary, smFRET-restrained molecular modelling provides a complementary method to crystallography and NMR for the structural determination of large, dynamic complexes, which often pose challenges to conventional approaches.

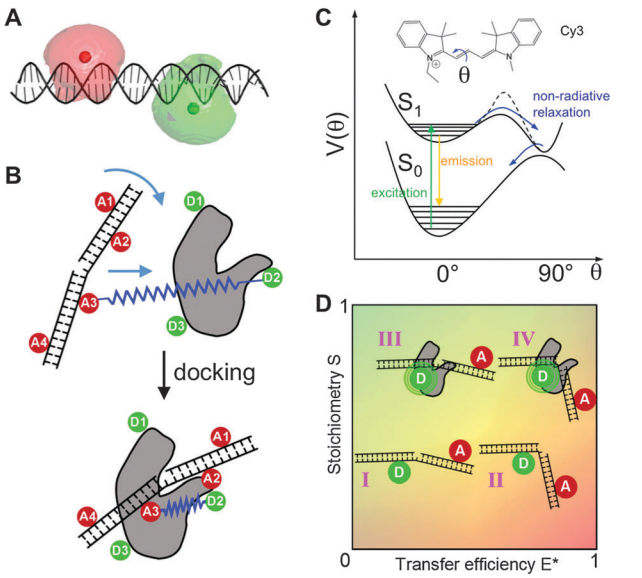

Fig. 6 New methods for ALEX. (A) A B-DNA duplex (black) with donor (green) and acceptor (red) showing mean dye positions (spheres) and their related accessible volumes (AVs) calculated using software from the Seidel lab and displayed using pymol.[39] (B) Rigid body docking schematic. Mean dye positions of all the donors (green) and acceptors (red) are determined by AV models and then fixed with respect to the corresponding labelled macromolecules, which are treated as rigid bodies. The experimentally determined distances are introduced as springs between these mean dye positions, for example between D2 and A3 (dark blue line), and the system is allowed to relax. (C) Chemical structure of the fluorophore Cy3 (Inset) and its potential energy surface (adapted from ref. 124, copyright (2007) National Academy of Sciences, U.S.A.). The dark blue arrows indicate a non-radiative relaxation process which is inhibited by the close proximity of a protein, presumably by increasing an energy barrier (dashed black line). (D) The effects of PIFE on the positions of various species in an *ES* histogram, unbound-unkinked DNA (I), unbound-kinked DNA (II), bound-unkinked DNA (III) and bound-kinked DNA (IV). The increased brightness of the donor due to PIFE is indicated by the concentric circles (species III and IV).

Protein-induced fluorescent enhancement (PIFE) and ALEX: PIFE-ALEX

PIFE is an assay in which the emission intensity of a single fluorescent dye attached to a DNA molecule provides information on the proximity or the conformational state of a protein interacting with DNA on the single-molecule level.[122] This is an attractive technique as dye conjugation to DNA is both simpler and more efficient than protein labelling, which requires many more complex steps for labelling and purification.

PIFE relies on using an environmentally sensitive dye, such as those from the cyanine series.[123] A common choice for single-molecule studies is Cy3, whose environmental sensitivity arises from the presence of a non-radiative relaxation pathway involving torsional motions of double bonds in the excited state (Fig. 6C). Constraints on this motion, due to either solvent viscosity (as was initially investigated[123]) or the close proximity of a protein,[124] increase the energy barrier to the non-radiative pathway (dashed line in Fig. 6C) and therefore increase the fluorescence quantum yield of the dye. Thus, binding and unbinding of a protein to a labelled nucleic acid can result in an increase and then a decrease in fluorescence intensity, respectively.

An early single-molecule application of this technique investigated the DNA binding of T7 DNA polymerase and subsequent conformational changes induced by the addition of a complementary nucleotide.[124] Fluorescence intensity histograms exhibited three distinct peaks, which were attributed to the unbound substrate and T7 bound in an open or closed conformation, respectively.

Hwang *et al.* investigated the distance dependence of the PIFE effect, using three different protein–nucleic acid systems,

BamH1, RIG-I and RecA.[122] Their results indicated that for these systems the PIFE effect exhibited a linear dependence on protein–dye distances in the 0 to 4 nm range, highly complementary to the FRET range. However, other systems appear to demonstrate less distance dependence, instead exhibiting an "all or nothing" effect, for example the binding of DNA polymerase I (Klenow fragment) to primer-template DNA.[125]

What can be gained from the combination of PIFE with ALEX smFRET? Let us consider the effect of PIFE on the position of species in the *ES* histogram arising from a DNA molecule labelled with an environmentally sensitive donor (Cy3) and a normal acceptor fluorophore (Fig. 6D – species I). Upon protein binding, the quantum yield of the donor increases, thereby increasing both $f_{D_{ex}}^{D_{em}}$ and $f_{D_{ex}}^{A_{em}}$. The $f_{A_{ex}}^{A_{em}}$ count, however, will be unaltered. Thus we will observe an increase in the stoichiometry (eqn (4)) and we obtain a ratiometric measure of PIFE, calculated relative to the fluorescence emission of the acceptor dye (Fig. 3D – species III). If a conformational change is also induced upon protein binding, a population with both increased *E* and *S* will be observed (Fig. 3D – species IV). This assay is therefore able to differentiate between the binding of a protein to a DNA substrate and any subsequent conformational change induced. It should be noted that there will also be an effect on the FRET efficiency even in the absence of any change in the inter-dye distance, due to the R_0 of the dye pair being dependent on the donor quantum yield (eqn (2)). Thus we would not recommend trying to determine accurate FRET distances with this assay. However, this method does open up the advantages of PIFE to confocal experiments, in which changes in the relative brightness of subspecies are often difficult to detect, but where changes in stoichiometry are more easily observed.

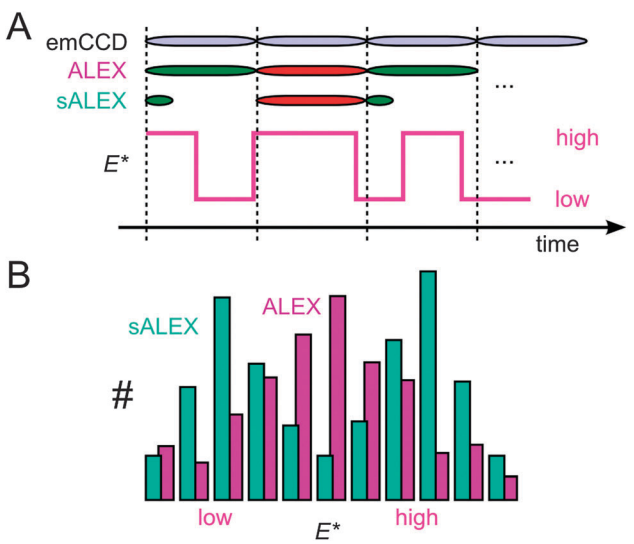

Fig. 7 Stroboscopic alternating-laser excitation (sALEX). (A) The achievable time resolution in imaging-based microscopy is limited by the frame rate of the camera (here emCCD). Whereas in conventional ALEX the fluorophores are excited for the entire time it takes to record a frame with the camera (ignoring the frame transfer time of the camera), the photons detected after excitation of the donor using the sALEX scheme represent a short snapshot from the underlying FRET behaviour here represented by a low or high FRET state. (B) As a result, the histogram of FRET values using sALEX allows resolving dynamic processes, which would have been averaged out in standard ALEX mode.

Stroboscopic ALEX (sALEX)

The two standard schemes for smFRET detection, solution-based confocal microscopy and TIRF microscopy, are ultimately limited in their ability to combine the parallel detection of many molecules with obtaining data at sufficiently high time resolution. The unliganded DNA polymerase I, as discussed above, exhibits fast conformational changes in the low millisecond time range.[62,63,65,66] These dynamics are too slow to directly resolve them using diffusion-based confocal microscopy and too fast to monitor them with conventional imaging-based microscopy, where the limit is imposed by the achievable frame rate of commercially available cameras with high sensitivity (as of 2013, the frame rate for full-frame detection is around 60 Hz for emCCD and 100 Hz for sCMOS devices). As a result, the apparent detectable FRET efficiency would represent an average of the underlying conformational dynamics. Faster frame rates can only be achieved by decreasing the active detection area or with additional pixel binning, thereby compromising the ability to monitor as many molecules as possible in parallel. To overcome these limitations, we propose a generalised scheme for imaging-based smFRET detection, sALEX, which combines the concepts of ALEX and stroboscopic illumination[126–128] to achieve a significant improvement in time resolution without sacrificing the highly parallelised detection (Fig. 7A). Instead of exciting the fluorophores for the full duration of a camera frame given by 1/(60 Hz) = 20 ms, the fluorophores in sALEX are excited for a short interval of, for example, 2 ms (Fig. 7B). Effectively, we take FRET-resolved snapshots of the enzyme conformation similar to the burst data obtained with diffusion-based confocal microscopy, but with hundreds of molecules in parallel. A requirement for sALEX is to surface-immobilise the molecules of interest. This is achieved using standard methods including using a biotin-streptavidin linkage to biotinylated PEG crafted on the glass surface,[129] by vesicle incapsulation[130,131] or by using a biotinylated, anti-His5/His6-tag antibody.[132] The achievable time-resolution is limited by the stability of the fluorophores and the excitation intensity, but we expect sub-millisecond time resolution to be feasible.

Conclusions

The last decade has seen tremendous advances in the field of single-molecule spectroscopy. More importantly, the development and refinement of the fluorescence-based toolkit is far from being over. Recent combinations of smFRET and computer-aided modelling will pave the way for elucidating biological structure and mechanism on the molecular level with the necessary time resolution to study dynamic processes within and between biological entities. In that respect, ALEX-based approaches offer important measures to monitor photophysics and to obtain the correction coefficients necessary for

the accurate determination of molecular distances. Additionally, we have suggested two new experimental variations of ALEX, which provide new ways to study multi-component interactions (PIFE-ALEX) and resolve faster dynamics using camera-based single-molecule detection (sALEX).

Acknowledgements

We thank Arjen Bader for critically reading the manuscript and providing helpful suggestions. T.D.C. was supported by the European Research Council [grant number 261227].

Notes and references

1 N. Walter, C. Huang, A. Manzo and M. Sobhy, *Nat. Methods*, 2008, **5**, 475–489.
2 C. Joo, H. Balci, Y. Ishitsuka, C. Buranachai and T. Ha, *Annu. Rev. Biochem.*, 2008, **77**, 51–76.
3 W. E. Moerner, *Proc. Natl. Acad. Sci. U. S. A.*, 2007, **104**, 12596–12602.
4 X. Xie, P. Choi, G. Li, N. Lee and G. Lia, *Annu. Rev. Biophys.*, 2008, **37**, 417–444.
5 B. Huang, M. Bates and X. Zhuang, *Annu. Rev. Biochem.*, 2009, **78**, 993–1016.
6 A. Robinson and A. M. van Oijen, *Nat. Rev. Microbiol.*, 2013, **11**, 303–315.
7 A. A. Deniz, S. Mukhopadhyay and E. A. Lemke, *J. R. Soc., Interface*, 2008, **5**, 15–45.
8 J. Hohlbein, K. Gryte, M. Heilemann and A. N. Kapanidis, *Phys. Biol.*, 2010, **7**, 031001.
9 H. Kim and T. Ha, *Rep. Prog. Phys.*, 2013, **76**, 016601.
10 A. N. Kapanidis, N. K. Lee, T. A. Laurence, S. Doose, E. Margeat and S. Weiss, *Proc. Natl. Acad. Sci. U. S. A.*, 2004, **101**, 8936–8941.
11 T. Ha, T. Enderle, D. F. Ogletree, D. S. Chemla, P. R. Selvin and S. Weiss, *Proc. Natl. Acad. Sci. U. S. A.*, 1996, **93**, 6264–6268.
12 K. Lymperopoulos, R. Crawford, J. P. Torella, M. Heilemann, L. C. Hwang, S. J. Holden and A. N. Kapanidis, *Angew. Chem., Int. Ed.*, 2010, **49**, 1316–1320.
13 T. Förster, *Anal. Phys.*, 1948, **2**, 55–75.
14 L. Stryer and R. Haugland, *Proc. Natl. Acad. Sci. U. S. A.*, 1967, **58**, 719–726.
15 T. Förster, *Naturwissenschaften*, 1946, **33**, 166–175.
16 B. W. van der Meer, *Rev. Mol. Biotechnol.*, 2002, **82**, 181–196.
17 A. Iqbal, S. Arslan, B. Okumus, T. J. Wilson, G. Giraud, D. G. Norman, T. Ha and D. M. J. Lilley, *Proc. Natl. Acad. Sci. U. S. A.*, 2008, **105**, 11176–11181.
18 J. R. Lakowicz, *Principles of Fluorescence Spectroscopy*, Springer, Berlin, 2006.
19 S. Nie, D. Chiu and R. Zare, *Science*, 1994, **266**, 1018–1021.
20 A. A. Deniz, M. Dahan, J. R. Grunwell, T. J. Ha, A. E. Faulhaber, D. S. Chemla, S. Weiss and P. G. Schultz, *Proc. Natl. Acad. Sci. U. S. A.*, 1999, **96**, 3670–3675.
21 D. Axelrod, *Biophotonics*, 2003, **361**, 1–33.
22 W. Moerner and D. Fromm, *Rev. Sci. Instrum.*, 2003, **74**, 3597–3619.
23 S. Preus and L. M. Wilhelmsson, *ChemBioChem*, 2012, 1990–2001.
24 S. Weiss, *Science*, 1999, **283**, 1676–1683.
25 R. Roy, S. Hohng and T. Ha, *Nat. Methods*, 2008, **5**, 507–516.
26 B. Schuler and W. Eaton, *Curr. Opin. Struct. Biol.*, 2008, **18**, 16–26.
27 C. Eggeling, S. Berger, L. Brand, J. R. Fries, J. Schaffer, A. Volkmer and C. A. M. Seidel, *J. Biotechnol.*, 2001, **86**, 163–180.
28 E. Nir, X. Michalet, K. M. Hamadani, T. A. Laurence, D. Neuhauser, Y. Kovchegov and S. Weiss, *J. Phys. Chem. B*, 2006, **110**, 22103–22124.
29 X. Michalet, R. A. Colyer, G. Scalia, A. Ingargiola, R. Lin, J. E. Millaud, S. Weiss, O. H. W. Siegmund, A. S. Tremsin, J. V. Vallerga, A. Cheng, M. Levi, D. Aharoni, K. Arisaka, F. Villa, F. Guerrieri, F. Panzeri, I. Rech, A. Gulinatti, F. Zappa, M. Ghioni and S. Cova, *Philos. Trans. R. Soc., B*, 2013, 368.
30 R. M. Clegg, *Methods Enzymol.*, 1992, **211**, 353–388.
31 E. Jares-Erijman and T. Jovin, *Nat. Biotechnol.*, 2003, **21**, 1387–1395.
32 E. Sisamakis, A. Valeri, S. Kalinin, P. J. Rothwell and C. A. M. Seidel, in *Methods in Enzymology*, ed. N. G. Walter, Academic Press, 2010, vol. 475, pp. 455–514.
33 A. N. Kapanidis, T. A. Laurence, N. K. Lee, E. Margeat, X. Kong and S. Weiss, *Acc. Chem. Res.*, 2005, **38**, 523–533.
34 N. K. Lee, A. N. Kapanidis, Y. Wang, X. Michalet, J. Mukhopadhyay, R. H. Ebright and S. Weiss, *Biophys. J.*, 2005, **88**, 2939–2953.
35 Y. Santoso, L. C. Hwang, L. Le Reste and A. N. Kapanidis, *Biochem. Soc. Trans.*, 2008, **36**, 738.
36 T. Laurence, X. Kong, M. Jager and S. Weiss, *Proc. Natl. Acad. Sci. U. S. A.*, 2005, **102**, 17348–17353.
37 B. K. Müller, E. Zaychikov, C. Bräuchle and D. C. Lamb, *Biophys. J.*, 2005, **89**, 3508–3522.
38 G. Vámosi, C. Gohlke and R. M. Clegg, *Biophys. J.*, 1996, **71**, 972–994.
39 S. Kalinin, T. Peulen, S. Sindbert, P. J. Rothwell, S. Berger, T. Restle, R. S. Goody, H. Gohlke and C. A. M. Seidel, *Nat. Methods*, 2012, **9**, 1218–1225.
40 A. Muschielok, J. Andrecka, A. Jawhari, F. Brückner, P. Cramer and J. Michaelis, *Nat. Methods*, 2008, **5**, 965–971.
41 U. B. Choi, P. Strop, M. Vrljic, S. Chu, A. T. Brunger and K. R. Weninger, *Nat. Struct. Mol. Biol.*, 2010, **17**, 318–324.
42 S. J. Holden, S. Uphoff, J. Hohlbein, D. Yadin, L. Le Reste, O. J. Britton and A. N. Kapanidis, *Biophys. J.*, 2010, **99**, 3102–3111.
43 A. N. Kapanidis, E. Margeat, S. O. Ho, E. Kortkhonjia, S. Weiss and R. H. Ebright, *Science*, 2006, **314**, 1144–1147.
44 L. M. Hsu, *Biochim. Biophys. Acta, Gene Struct. Expression*, 2002, **1577**, 191–207.
45 A. J. Carpousis and J. D. Gralla, *J. Mol. Biol.*, 1985, **183**, 165–177.

46 D. C. Straney and D. M. Crothers, *J. Mol. Biol.*, 1987, **193**, 267–278.
47 B. Krummel and M. J. Chamberlin, *Biochemistry*, 1989, **28**, 7829–7842.
48 M. Pal, A. S. Ponticelli and D. S. Luse, *Mol. Cell*, 2005, **19**, 101–110.
49 T. Cordes, Y. Santoso, A. I. Tomescu, K. Gryte, L. C. Hwang, B. Camará, S. Wigneshweraraj and A. N. Kapanidis, *Biochemistry*, 2010, **49**, 9171–9180.
50 N. C. Robb, T. Cordes, L. C. Hwang, K. Gryte, D. Duchi, T. D. Craggs, Y. Santoso, S. Weiss, R. H. Ebright and A. N. Kapanidis, *J. Mol. Biol.*, 2013, **425**, 875–885.
51 A. Chakraborty, D. Wang, Y. W. Ebright, Y. Korlann, E. Kortkhonjia, T. Kim, S. Chowdhury, S. Wigneshweraraj, H. Irschik, R. Jansen, B. T. Nixon, J. Knight, S. Weiss and R. H. Ebright, *Science*, 2012, **337**, 591–595.
52 A. Chakraborty, D. Wang, Y. W. Ebright and R. H. Ebright, *Methods Enzymol.*, 2010, **472**, 19–30.
53 S. Milles, S. Tyagi, N. Banterle, C. Koehler, V. VanDelinder, T. Plass, A. P. Neal and E. A. Lemke, *J. Am. Chem. Soc.*, 2012, **134**, 5187–5195.
54 C. C. Liu and P. G. Schultz, *Annu. Rev. Biochem.*, 2010, **79**, 413–444.
55 M. Antonik, S. Felekyan, A. Gaiduk and C. A. M. Seidel, *J. Phys. Chem. B*, 2006, **110**, 6970–6978.
56 S. Kalinin, S. Felekyan, M. Antonik and C. A. M. Seidel, *J. Phys. Chem. B*, 2007, **111**, 10253–10262.
57 S. Kalinin, S. Felekyan, A. Valeri and C. A. M. Seidel, *J. Phys. Chem. B*, 2008, **112**, 8361–8374.
58 S. Kalinin, A. Valeri, M. Antonik, S. Felekyan and C. A. M. Seidel, *J. Phys. Chem. B*, 2010, **114**, 7983–7995.
59 I. V. Gopich and A. Szabo, *J. Phys. Chem. B*, 2010, **114**, 15221–15226.
60 T. E. Tomov, R. Tsukanov, R. Masoud, M. Liber, N. Plavner and E. Nir, *Biophys. J.*, 2012, **102**, 1163–1173.
61 X. Kong, E. Nir, K. Hamadani and S. Weiss, *J. Am. Chem. Soc.*, 2007, **129**, 4643–4654.
62 J. P. Torella, S. J. Holden, Y. Santoso, J. Hohlbein and A. N. Kapanidis, *Biophys. J.*, 2011, **100**, 1568–1577.
63 Y. Santoso, J. P. Torella and A. N. Kapanidis, *ChemPhysChem*, 2010, **11**, 2209–2219.
64 S. Felekyan, H. Sanabria, S. Kalinin, R. Kühnemuth and C. A. M. Seidel, in *Methods in Enzymology*, ed. S. Y. Tetin, Academic Press, 2013, vol. 519, pp. 39–85.
65 Y. Santoso, C. M. Joyce, O. Potapova, L. Le Reste, J. Hohlbein, J. P. Torella, N. D. F. Grindley and A. N. Kapanidis, *Proc. Natl. Acad. Sci. U. S. A.*, 2010, **107**, 715–720.
66 J. Hohlbein, L. Aigrain, T. D. Craggs, O. Bermek, O. Potapova, P. Shoolizadeh, N. D. F. Grindley, C. M. Joyce and A. N. Kapanidis, *Nat. Commun.*, 2013, **4**, 2131.
67 S. J. Johnson, J. S. Taylor and L. S. Beese, *Proc. Natl. Acad. Sci. U. S. A.*, 2003, **100**, 3895–3900.
68 E. Y. Wu and L. S. Beese, *J. Biol. Chem.*, 2011, **286**, 19758–19767.
69 K. A. Henzler-Wildman, V. Thai, M. Lei, M. Ott, M. Wolf-Watz, T. Fenn, E. Pozharski, M. A. Wilson, G. A. Petsko, M. Karplus, C. G. Hubner and D. Kern, *Nature*, 2007, **450**, 838–844.
70 D. S. Majumdar, I. Smirnova, V. Kasho, E. Nir, X. Kong, S. Weiss and H. R. Kaback, *Proc. Natl. Acad. Sci. U. S. A.*, 2007, **104**, 12640–12645.
71 R. P. Goodman, M. Heilemann, S. Doose, C. M. Erben, A. N. Kapanidis and A. J. Turberfield, *Nat. Nanotechnol.*, 2008, **3**, 93–96.
72 A. Y. Kobitski, M. Hengesbach, M. Helm and G. U. Nienhaus, *Angew. Chem., Int. Ed.*, 2008, **47**, 4326–4330.
73 W. J. A. Koopmans, R. Buning, T. Schmidt and J. van Noort, *Biophys. J.*, 2009, **97**, 195–204.
74 R. Masoud, R. Tsukanov, T. E. Tomov, N. Plavner, M. Liber and E. Nir, *ACS Nano*, 2012, **6**, 6272–6283.
75 S. Doose, M. Heilemann, X. Michalet, S. Weiss and A. N. Kapanidis, *Eur. Biophys. J. Biophys. Lett.*, 2007, **36**, 669–674.
76 J. Hendrix and D. C. Lamb, in *Methods in Enzymology*, ed. S. Y. Tetin, Academic Press, 2013, vol. 518, pp. 205–243.
77 Y. H. Foo, N. Naredi-Rainer, D. C. Lamb, S. Ahmed and T. Wohland, *Biophys. J.*, 2012, **102**, 1174–1183.
78 K. Mapa, M. Sikor, V. Kudryavtsev, K. Waegemann, S. Kalinin, C. A. M. Seidel, W. Neupert, D. C. Lamb and D. Mokranjac, *Mol. Cell*, 2010, **38**, 89–100.
79 P. Rothwell, S. Berger, O. Kensch, S. Felekyan, M. Antonik, B. Wohrl, T. Restle, R. Goody and C. Seidel, *Proc. Natl. Acad. Sci. U. S. A.*, 2003, **100**, 1655–1660.
80 J. Widengren, V. Kudryavtsev, M. Antonik, S. Berger, M. Gerken and C. A. M. Seidel, *Anal. Chem.*, 2006, **78**, 2039–2050.
81 V. Kudryavtsev, M. Sikor, S. Kalinin, D. Mokranjac, C. A. M. Seidel and D. C. Lamb, *ChemPhysChem*, 2012, **13**, 1060–1078.
82 L. Olofsson and E. Margeat, *Opt. Express*, 2013, **21**, 3370–3378.
83 J. Ross, P. Buschkamp, D. Fetting, A. Donnermeyer, C. M. Roth and P. Tinnefeld, *J. Phys. Chem. B*, 2007, **111**, 321–326.
84 S. W. Yim, T. Kim, T. A. Laurence, S. Partono, D. Kim, Y. Kim, S. Weiss and A. Reitmair, *Clin. Chem.*, 2012, **58**, 707–716.
85 I. H. Stein, C. Steinhauer and P. Tinnefeld, *J. Am. Chem. Soc.*, 2011, **133**, 4193–4195.
86 S. Kim, A. M. Streets, R. R. Lin, S. R. Quake, S. Weiss and D. S. Majumdar, *Nat. Methods*, 2011, **8**, 242–245.
87 H. Li, L. Ying, J. J. Green, S. Balasubramanian and D. Klenerman, *Anal. Chem.*, 2003, **75**, 1664–1670.
88 A. Pertsinidis, Y. Zhang and S. Chu, *Nature*, 2010, **466**, 647–651.
89 A. Orte, R. W. Clarke and D. Klenerman, *ChemPhysChem*, 2011, **12**, 491–499.
90 T. D. Harris, P. R. Buzby, H. Babcock, E. Beer, J. Bowers, I. Braslavsky, M. Causey, J. Colonell, J. DiMeo, J. W. Efcavitch, E. Giladi, J. Gill, J. Healy, M. Jarosz,

D. Lapen, K. Moulton, S. R. Quake, K. Steinmann, E. Thayer, A. Tyurina, R. Ward, H. Weiss and Z. Xie, *Science*, 2008, **320**, 106–109.
91 E. Margeat, A. N. Kapanidis, P. Tinnefeld, Y. Wang, J. Mukhopadhyay, R. H. Ebright and S. Weiss, *Biophys. J.*, 2006, **90**, 1419–1431.
92 I. Rasnik, S. McKinney and T. Ha, *Nat. Methods*, 2006, **3**, 891–893.
93 J. Vogelsang, R. Kasper, C. Steinhauer, B. Person, M. Heilemann, M. Sauer and P. Tinnefeld, *Angew. Chem., Int. Ed.*, 2008, **47**, 5465–5469.
94 T. Ha and P. Tinnefeld, *Annu. Rev. Phys. Chem.*, 2012, **63**, 595–617.
95 N. K. Lee, A. N. Kapanidis, H. R. Koh, Y. Korlann, S. O. Ho, Y. Kim, N. Gassman, S. K. Kim and S. Weiss, *Biophys. J.*, 2007, **92**, 303–312.
96 S. Lee, J. Lee and S. Hohng, *PLoS One*, 2010, **5**, e12270.
97 J. Lee, S. Lee, K. Ragunathan, C. Joo, T. Ha and S. Hohng, *Angew. Chem., Int. Ed.*, 2010, **49**, 9922–9925.
98 M. A. Sobhy, M. M. Elshenawy, M. Takahashi, B. H. Whitman, N. G. Walter and S. M. Hamdan, *Rev. Sci. Instrum.*, 2011, **82**, 113702.
99 J. Vogelsang, T. Cordes, C. Forthmann, C. Steinhauer and P. Tinnefeld, *Proc. Natl. Acad. Sci. U. S. A.*, 2009, **106**, 8107–8112.
100 J. Vogelsang, T. Cordes and P. Tinnefeld, *Photochem. Photobiol. Sci.*, 2009, **8**, 486–496.
101 T. Cordes, J. Vogelsang, M. Anaya, C. Spagnuolo, A. Gietl, W. Summerer, A. Herrmann, K. Müllen and P. Tinnefeld, *J. Am. Chem. Soc.*, 2010, **132**, 2404–2409.
102 J. Vogelsang, T. Cordes, C. Forthmann, C. Steinhauer and P. Tinnefeld, *Nano Lett.*, 2010, **10**, 672–679.
103 S. Uphoff, S. Holden, L. Le Reste, J. Periz, S. van de Linde, M. Heilemann and A. Kapanidis, *Nat. Methods*, 2010, **7**, 831–836.
104 S. Uphoff, K. Gryte, G. Evans and A. N. Kapanidis, *ChemPhysChem*, 2011, **12**, 571–579.
105 L. Le Reste, J. Hohlbein, K. Gryte and A. N. Kapanidis, *Biophys. J.*, 2012, **102**, 2658–2668.
106 J. Chen, A. Tsai, A. Petrov and J. D. Puglisi, *J. Am. Chem. Soc.*, 2012, **134**, 5734–5737.
107 J. J. Schwartz and S. R. Quake, *Proc. Natl. Acad. Sci. U. S. A.*, 2009, **106**, 20294–20299.
108 J. N. M. Pinkney, P. Zawadzki, J. Mazuryk, L. K. Arciszewska, D. J. Sherratt and A. N. Kapanidis, *Proc. Natl. Acad. Sci. U. S. A.*, 2012, **109**, 20871–20876.
109 C. Chen, H. Zhang, S. L. Broitman, M. Reiche, I. Farrell, B. S. Cooperman and Y. E. Goldman, *Nat. Struct. Mol. Biol.*, 2013, **20**, 582–588.
110 C. Chen, B. Stevens, J. Kaur, D. Cabral, H. Liu, Y. Wang, H. Zhang, G. Rosenblum, Z. Smilansky, Y. E. Goldman and B. S. Cooperman, *Mol. Cell*, 2011, **42**, 367–377.
111 B. Stevens, C. Chen, I. Farrell, H. Zhang, J. Kaur, S. L. Broitman, Z. Smilansky, B. S. Cooperman and Y. E. Goldman, *PLoS One*, 2012, **7**, e38344.
112 C. Ratzke, F. Berkemeier and T. Hugel, *Proc. Natl. Acad. Sci. U. S. A.*, 2011, **109**, 161–166.
113 T. D. Craggs and A. N. Kapanidis, *Nat. Methods*, 2012, **9**, 1157–1158.
114 A. T. Brunger, P. Strop, M. Vrljic, S. Chu and K. R. Weninger, *J. Struct. Biol.*, 2011, **173**, 497–505.
115 V. Mekler, E. Kortkhonjia, J. Mukhopadhyay, J. Knight, A. Revyakin, A. N. Kapanidis, W. Niu, Y. W. Ebright, R. Levy and R. H. Ebright, *Cell*, 2002, **108**, 599–614.
116 J. Andrecka, R. Lewis, F. Brückner, E. Lehmann, P. Cramer and J. Michaelis, *Proc. Natl. Acad. Sci. U. S. A.*, 2008, **105**, 135–140.
117 A. K. Woźniak, G. F. Schröder, H. Grubmüller, C. A. M. Seidel and F. Oesterhelt, *Proc. Natl. Acad. Sci. U. S. A.*, 2008, **105**, 18337–18342.
118 J. J. McCann, L. Zheng, S. Chiantia and M. E. Bowen, *Structure*, 2011, **19**, 810–820.
119 J. J. McCann, L. Zheng, D. Rohrbeck, S. Felekyan, R. Kühnemuth, R. B. Sutton, C. A. M. Seidel and M. E. Bowen, *Proc. Natl. Acad. Sci. U. S. A.*, 2012, **109**, 15775–15780.
120 A. Muschielok and J. Michaelis, *J. Phys. Chem. B*, 2011, **115**, 11927–11937.
121 S. Sindbert, S. Kalinin, H. Nguyen, A. Kienzler, L. Clima, W. Bannwarth, B. Appel, S. Müller and C. A. M. Seidel, *J. Am. Chem. Soc.*, 2011, **133**, 2463–2480.
122 H. Hwang, H. Kim and S. Myong, *Proc. Natl. Acad. Sci. U. S. A.*, 2011, **108**, 7414–7418.
123 P. F. Aramendia, R. M. Negri and E. S. Roman, *J. Phys. Chem.*, 1994, **98**, 3165–3173.
124 G. Luo, M. Wang, W. H. Konigsberg and X. S. Xie, *Proc. Natl. Acad. Sci. U. S. A.*, 2007, **104**, 12610–12615.
125 R. P. Markiewicz, K. B. Vrtis, D. Rueda and L. J. Romano, *Nucleic Acids Res.*, 2012, **40**, 7975–7984.
126 J. Elf, G.-W. Li and X. S. Xie, *Science*, 2007, **316**, 1191–1194.
127 C. Flors, J. Hotta, H. Uji-i, P. Dedecker, R. Ando, H. Mizuno, A. Miyawaki and J. Hofkens, *J. Am. Chem. Soc.*, 2007, **129**, 13970–13977.
128 S. Blumberg, A. Gajraj, M. W. Pennington and J.-C. Meiners, *Biophys. J.*, 2005, **89**, 1272–1281.
129 R. Lamichhane, A. Solem, W. Black and D. Rueda, *Methods*, 2010, **52**, 192–200.
130 B. Okumus, T. J. Wilson, D. M. J. Lilley and T. Ha, *Biophys. J.*, 2004, **87**, 2798–2806.
131 E. Boukobza, A. Sonnenfeld and G. Haran, *J. Phys. Chem. B*, 2001, **105**, 12165–12170.
132 R. Zhou, S. Kunzelmann, M. R. Webb and T. Ha, *Nano Lett.*, 2011, **11**, 5482–5488.